Gyrokinetic study of slowing-down α particles transport due to trapped electron mode turbulence

S.M. Yang,[1] C. Angioni,[2] T.S. Hahm,[1, a)] D.H. Na,[1] and Y.S. Na[1]

[1)] *Department of Nuclear Engineering, Seoul National University, Seoul 08826, Republic of Korea*

[2)] *Max-Planck-Institut für Plasmaphysik, D-85748 Garching bei München, Germany*

(Dated: 20 September 2018)

Transport of α particles due to trapped electron mode (TEM) turbulence is investigated from nonlinear and quasilinear gyrokinetic simulations. We consider both slowing-down and Maxwellian distribution functions for α particles, and identify and compare diffusive and convective parts of α particle transport as a function of the α particle's energy normalized to the background plasma temperature. We find that TEM induces much lower transport of energetic α particles such as fusion products than that of thermal Helium ions in the trace limit. This disparity from our study is found to be even greater than that reported previously for ion temperature gradient (ITG) mode [C. Angioni and A.G. Peeters, Phys.Plasmas. **15**, 052307 (2008)].

[a)] tshahm@snu.ac.kr

I. INTRODUCTION

Transport of energetic particles (EPs) by turbulence is a subject of both magnetic fusion relevance such as a successful operation of ITER[1] and scientific interest. Excitation of various Alfvénic instabilities by EPs and their impact on EPs transport have been extensively studied in the past and recently reviewed, for instance, in Ref. 2. Even in the absence of EP-driven Alfvénic instabilities and of large scale magnetohydrodynamic (MHD) instabilities, tokamak plasma confinement has been limited by the anomalous transport due to turbulence developed from various microinstabilities.[3,4]

In this paper, we investigate transport of α particles in the presence of collisionless trapped electron mode (TEM) turbulence in tokamak plasmas. Linear properties of collisionless trapped electron mode can be found in Ref. 5. We consider α particles with a slowing-down distribution function[6] and background ions and electrons with Maxwellian distribution functions. Their dynamics is described by the electrostatic nonlinear gyrokinetic equation in toroidal geometry[7,8] and simulated using the GKW code.[9] Previous gyrokinetic studies on slowing-down α particles transport due to electrostatic turbulence have considered ion temperature gradient (ITG) mode turbulence.[10–13] Prior to that study, there have been numerous publications on EP transport due to ITG turbulence using Maxwellian distribution function for α particles.[14] We note that TEM is a prime contributor to core microturbulence and anomalous transport of tokamak plasmas alongside ITG. Depending on plasma parameters, either one can be dominant or two can coexist with a comparable strength. In this paper, we consider fusion product α particles continuously born at 3.5

MeV and being slowed down due to Coulomb collisions with electrons. We also consider α-particles with Maxwellian distribution with the same average energy for elucidation of physical trends. In addition, we investigate the dependence of α particles transport on their energy E_α normalized to T_e. In most cases, α particles can be treated as tracers due to their small effect on TEM turbulence for n_α/n_e up to 10 %.

Principal results of this paper are as follows.

i) Transport of α particles with high energy is significantly smaller than the thermal He transport. This reduction is even stronger than that for ITG,[10] due to shorter size of TEM in the direction perpendicular to the magnetic field.

ii) Pure convection of α particles from nonlinear simulation is outward, with the convection to diffusion ratio RV_{pk}/D_α decreasing with E_α/T_e.

iii) k_θ spectrum of $\left|\frac{\delta n}{n_0}\right|^2$ at nonlinear saturation exhibits a peak at $k_\theta\rho_i \simeq 0.4$ and a decay for shorter wavelengths. These are similar to results from measurement on Tore Supra Ohmic plasmas[15] and from a weak turbulence theory based on nonlinear gyrokinetic equation.[16]

The rest of this paper is organized as follows. In Sec. II, we briefly introduce the theoretical model and its implementation for GKW simulation. In Sec III, diffusive and convective components computed with the linear TEM GKW calculations are shown. Nonlinear GKW calculations are presented in Sec IV. In particular, k-spectrum and saturated amplitude are compared to the theory predictions. Conclusions are drawn in Sec V. Finally, a short derivation of the nonlinear gyrokinetic Vlasov equation for arbitrary isotropic equilibrium distribution function used in simulations from the modern gyrokinetic equation[8] is presented in the Appendix.

II. THEORETICAL MODEL

Our theoretical model consists of the electrostatic nonlinear gyrokinetic description of α particles, working gas ions, and electrons in toroidal geometry. A slowing-down equilibrium distribution function is considered for α particles and the $E \times B$ nonlinearity is kept for all species. We perform gyrokinetic simulations using the GKW code.[9] The code solves the electromagnetic gyrokinetic equation. In the electrostatic limit, its updated version[10] solves the following nonlinear toroidal gyrokinetic Vlasov equations in the electrostatic limit,

$$\frac{\partial \delta f}{\partial t} + \frac{c\mathbf{b} \times \boldsymbol{\nabla} \left(\langle \delta \phi \rangle \right)}{B} \cdot \boldsymbol{\nabla} \delta f + \left(v_{\parallel} \mathbf{b} + \mathbf{v_D} \right) \cdot \boldsymbol{\nabla} \delta f - \frac{\mathbf{b}}{m} \cdot \left(\mu \boldsymbol{\nabla} B_0 \right) \frac{\partial \delta f}{\partial v_{\parallel}} = S, \tag{1}$$

where S is given by

$$S = - \left(\frac{c\mathbf{b} \times \boldsymbol{\nabla} \left(\langle \delta \phi \rangle \right)}{B} + \mathbf{v_D} \right) \cdot \boldsymbol{\nabla}_{\boldsymbol{p}} F_0 + \left(v_{\parallel} \mathbf{b} + \mathbf{v_D} \right) \cdot \left(Zq \boldsymbol{\nabla} \langle \delta \phi \rangle \right) \frac{\partial F_0}{\partial E}. \tag{2}$$

In (1) and (2), Z and q are the particle charge number and the elementary charge, $v_{\parallel}$ is the parallel velocity, T is the temperature, $\mathbf{b}$ is the unit vector aligned with equilibrium magnetic field $B\mathbf{b}$, m is the mass, μ is the magnetic moment, and $\delta\phi$ is the perturbed potential. The bracket $\langle\rangle$ indicates the gyro-phase average and $\boldsymbol{\nabla}_{\boldsymbol{p}}$ means that only $\boldsymbol{\nabla} n_0$, $\boldsymbol{\nabla} T_0$ terms of $\boldsymbol{\nabla} F_0$ are considered. This can be derived from the modern conservative nonlinear gyrokinetic equation[8] using justifiable simplifications as detailed in the Appendix. We note that there is an independent derivation of the electromagnetic nonlinear gyrokinetic equation using a different method and different variables[13] starting from Ref. 17. The second term on the LHS represents the dominant $E \times B$ nonlinearity. The terms related to the parallel velocity space nonlinearity, the equilibrium $E \times B$ shear[18] and plasma rotation[19,20] are not included

in equations (1), (2) which are beyond the scope of this study. Equation (1) is solved with the corresponding gyrokinetic Poisson equation in Fourier space.

For background main ions and electrons, a Maxwellian distribution $F_0 = F_M$ can be used for the equilibrium distribution given as,

$$F_M = \frac{n_0}{\pi^{3/2} v_{th}^3} e^{-v^2/v_{th}^2} \tag{3}$$

where $v_{th}^2 = 2T/m$, following normalization of Ref. 10 and n_0 is the equilibrium density. For energetic α particles with $E_\alpha/T_e >> 1$, equilibrium distribution can be approximated by a slowing-down distribution function $F_0 = F_s$[14], rather than Maxwellian distribution, namely

$$F_0 = \frac{3n_0}{4\pi ln\left(v_\alpha^3/v_c^3 + 1\right)} \frac{H\left(v_\alpha - v\right)}{v_c^3 + v^3}. \tag{4}$$

In Eq. (4), v_α is the maximum fast particle velocity at birth given by $E_\alpha = m_\alpha v_\alpha^2/2 = 3.5MeV$, and v_c is the slowing down critical velocity given by

$$v_c^3 = \frac{3\sqrt{\pi}}{4} \frac{m_e}{m_\alpha} Z_I v_{the}^3, \tag{5}$$

where effective charge $Z_I = m_\alpha \sum_i n_i (Z_i^2/m_i)/n_e$ is weighted over the ion mass. $Z_I = 5/3$, for 50% D and 50% T mixture considered in this work. Analytic progress and description for slowing-down distribution function F_0 in Eqs. (1) and (2) become feasible with a gyrokinetic formulation with $E = mv^2/2$ and μ as independent velocity space variables rather than $v_\parallel$ and μ is useful. Then, the linearized gyro-kinetic equation[21] can be written in the simplified form for a single toroidal mode in the ballooning representation for an $s - \alpha$ equilibrium[22] as in Ref. 10.

$$\frac{\partial \hat{g}_\alpha}{\partial t} + \frac{v_\parallel}{q_s R} \frac{\partial \hat{g}_\alpha}{\partial \theta} + i\omega_{d\alpha} \hat{g}_\alpha = \frac{e_\alpha}{E_\alpha} F_{s\alpha} J_0 \left[H_s\left(\dot{E}\right) \frac{\partial \hat{\phi}\left(\theta\right)}{\partial t} + i\omega_{S*} \hat{\phi}\left(\theta\right) \right], \tag{6}$$

where q_s is the safety factor, R is the major radius, θ is the extended poloidal angle and $\dot{E} = E/E_\alpha$. $\omega_{d\alpha}$ can be given as

$$\omega_{d\alpha} = \frac{k_\theta E_\alpha}{e_\alpha BR}\left(\frac{E}{T_\alpha}\right)\left(1+\frac{v_\parallel^2}{v^2}\right)\left(cos\theta + \left[\hat{s}\theta - \alpha sin\theta\right] sin\theta\right) \tag{7}$$

and slowing-down diamagnetic frequency is defined as

$$\omega_{S*} = \frac{k_\theta E_\alpha}{e_\alpha BR}\left[\frac{R}{L_{n\alpha}} + K_s\left(\dot{E}\right)\frac{R}{L_{E_c}}\right]. \tag{8}$$

With this normalization, real frequency of the most unstable mode ω_r becomes positive for ITG modes and negative for TEM[23], which is opposite to more traditional definition.[4]

A non-adiabatic part of the perturbed distribution function $\hat{g}_\alpha$ is related to the perturbed distribution function $\hat{f}_\alpha$ by

$$\hat{g}_\alpha = \hat{f}_\alpha + e_\alpha F_{s_\alpha} H_s\left(\dot{E}\right)\hat{\phi}\left(\theta\right). \tag{9}$$

The derivatives of the distribution function are given as following form for the slowing down distribution function

$$H_s\left(\dot{E}\right) = -\frac{dln\left(F_s\right)}{d\dot{E}} = \frac{3}{2}\frac{\dot{E}^{0.5}}{\dot{E}^{1.5}+\dot{E}_c^{0.5}}, \tag{10}$$

and

$$K_s\left(\dot{E}\right) = -\frac{3}{2}\left[\frac{1}{ln\left(1/\dot{E}_c^{1.5}+1\right)+\left(1+\dot{E}_c^{1.5}\right)} - \frac{\dot{E}_c^{0.5}}{\dot{E}^{1.5}+\dot{E}_c^{0.5}}\right]. \tag{11}$$

The gyrokinetic equation with an equivalent Maxwellian distribution can be obtained by replacing E_α with T_α, H_S with H_M and K_S with K_M in Eq. (6), where H_M and K_M can be written as,

$$H_M\left(\dot{E}\right) = -\frac{dln\left(F_M\right)}{d\dot{E}} = 1, \tag{12}$$

and

$$K_M\left(\dot{E}\right) = \left(\dot{E} - \frac{3}{2}\right)\frac{dlnT_\alpha}{dlnE_c}. \tag{13}$$

The GKW code has been modified to include the slowing down distribution for energetic particle transport.[10] A detailed benchmarking between GKW and GS2 has also been carried out in Ref. 10. In addition, a benchmarking between GKW, GS2 and GENE has been performed in Ref. 13.

The linearized equation Eq. (6) for α particles can be expressed in terms of Fourier representation $e^{i(kx-\omega t)}$ where $\omega = \omega_r + i\gamma$ is the complex eigenfrequency,

$$-i\omega\hat{g}_\alpha + \frac{v_\parallel}{qR}\frac{\partial\hat{g}_\alpha}{\partial\theta} + i\omega_{d\alpha}\hat{g}_\alpha = \frac{e_\alpha\omega_{D\alpha}}{E_\alpha}F_\alpha J_0\hat{\phi}\left[\frac{R}{L_{n\alpha}} + K_s\left(\dot{E}\right)\frac{R}{L_{Ec}} - \frac{\omega}{\omega_{D\alpha}}H_s\left(\dot{E}\right)\right]. \tag{14}$$

The solution of $\hat{g}_\alpha$ can be expressed in the form

$$\hat{g}_\alpha = \frac{e_\alpha}{E_\alpha}F_\alpha J_0\hat{\phi}\frac{-\omega_{D\alpha}}{\omega - k_\parallel v_\parallel - \omega_{d\alpha}}\left[\frac{R}{L_{n\alpha}} + K_s\left(\dot{E}\right)\frac{R}{L_{Ec}} - \frac{\omega}{\omega_{D\alpha}}H_s\left(\dot{E}\right)\right], \tag{15}$$

where we define the energy dependent drift frequency $\omega_{D\alpha} = \left(k_\theta E_\alpha\right)/\left(e_\alpha BR\right)$ for the normalization purposes. By integrating $\hat{g}_\alpha$ over the velocity space, the non-adiabatic part of the density perturbation $\tilde{n}_{n.a.}$ can be obtained as

$$\begin{aligned}\tilde{n}_{n.a.} =& \frac{e_\alpha}{E_\alpha}\left[\left\{\int\left(\frac{-F_\alpha J_0^2}{\omega - k_\parallel v_\parallel - \omega_{d\alpha}}d^3\mathbf{v}\right)\omega_{D\alpha}\hat{\phi}\right\}\frac{R}{L_{n\alpha}}\right.\\ &+\left\{\int\left(\frac{-K_s\left(\dot{E}\right)F_\alpha J_0^2}{\omega - k_\parallel - \omega_{d\alpha}}d^3\mathbf{v}\right)\omega_{D_\alpha}\hat{\phi}\right\}\frac{R}{L_{Ec}}\\ &\left.-\left\{\int\left(\frac{-H_s\left(\dot{E}\right)F_\alpha J_0^2}{\omega - k_\parallel - \omega_{d\alpha}}d^3\mathbf{v}\right)\omega_{D_\alpha}\hat{\phi}\right\}\frac{\omega}{\omega_{D\alpha}}\right].\end{aligned} \tag{16}$$

The quasilinear radial particle flux, which is proportional to the cross-correlation between density and radial component of $E\times B$ velocity fluctuation can be given as $\Gamma_k =$

$\langle \delta v_E \delta n \rangle_{FSA} = \langle Im\left(k_\theta \delta\phi^\dagger \delta n/B\right)\rangle_{FSA}$ where the symbol † indicates the complex conjugate and the bracket $\langle\rangle_{FSA}$ indicates the flux surface average. By Eq. (16), quasilinear particle flux for a given wave number k_θ can be written in the form,

$$\frac{R\Gamma_k}{n_\alpha} = D_k \frac{R}{L_{n\alpha}} + D_{Ek}\frac{R}{L_{Ec}} + RV_{pk}, \tag{17}$$

where

$$D_k = \left\langle \frac{Rk_\theta}{n_\alpha B}\frac{e_\alpha}{E_\alpha} Im\left\{\int\left(\frac{-F_\alpha J_0^2}{\omega - k_\parallel v_\parallel - \omega_{d\alpha}} d^3\mathbf{v}\right)\omega_{D\alpha}\hat{\phi}\hat{\phi}^\dagger\right\}\right\rangle_{FSA}, \tag{18}$$

$$D_{Ek} = \left\langle \frac{Rk_\theta}{n_\alpha B}\frac{e_\alpha}{E_\alpha} Im\left\{\int\left(\frac{-K_s\left(dotE\right)F_\alpha J_0^2}{\omega - k_\parallel v_\parallel - \omega_{d\alpha}} d^3\mathbf{v}\right)\omega_{D\alpha}\hat{\phi}\hat{\phi}^\dagger\right\}\right\rangle_{FSA}, \tag{19}$$

$$RV_{pk} = \left\langle \frac{Rk_\theta}{n_\alpha B}\frac{e_\alpha}{E_\alpha}\frac{1}{\omega_{D\alpha}} Im\left\{\omega\int\left(\frac{-H_s\left(dotE\right)F_\alpha J_0^2}{\omega - k_\parallel v_\parallel - \omega_{d\alpha}} d^3\mathbf{v}\right)\omega_{D\alpha}\hat{\phi}\hat{\phi}^\dagger\right\}\right\rangle_{FSA}. \tag{20}$$

It is useful to define the following coefficients $C_{E\alpha} = D_{EK}/D_k$ and $C_{pk} = RV_{pk}/D_k$, which are convective contributions that determine the α particle flux. We shall call $C_{E\alpha}$ the thermodiffusion coefficient, and C_{pk} the pure convection coefficient. These derivations follow Ref. 10 and Eqs. (18) and (19) appear also in the Ref. 10. However, an error in Eq. (25) of Ref. 10 has been corrected in Eq. (20). This correction is not important to ITG dominant case with $\omega_r > 0$ considered in Ref. 10. On the other hand, for the TEM dominant case with $\omega_r < 0$, this correction is important in determining the sign of the pinch term. Accordingly, Eq. (29) in the Ref. 10 should read

$$RV_{pk} = -\frac{1}{n_\alpha}\frac{1}{\omega_{D\alpha}}\int G_{Vpk}\left(E\right)F_\alpha H\left(\dot{E}\right)\left(2\pi\sqrt{E}\right)dE, \tag{21}$$

with

$$G_{Vpk} = \left\langle \frac{Rk_\theta}{n_\alpha B}\frac{e_\alpha\omega_{D\alpha}}{E_\alpha} Im\left\{\omega\int 1\frac{Bd\lambda}{\sqrt{2\left(1-\lambda B\right)}} J_0 h_D \hat{\phi}^\dagger\right\}\right\rangle_{FSA}. \tag{22}$$

III. RESULTS FROM LINEAR SIMULATIONS

The main parameters used in the simulations are chosen for TEM dominant case: $r/a = 0.5$, $R/a = 3$, $q = 1.4$, $s = 0.8$, $T_e = T_i$, $R/L_{Ti} = 2.2$, $R/L_{Te} = 6.9$ and $R/L_n = 2.2$. We consider a collisionless plasma in $s - \alpha$ geometry. The parameters are based on the CYCLONE case,[24] except for the fact that a weaker ion temperature gradient is chosen to focus on TEM rather than ITG.[25] Several studies have shown that those parameters can present TEM modes well at wavelength, $k_\theta \rho_i \lesssim 1$.[25,26] ETG modes can also be linearly unstable for these parameters at shorter wavelengths, with poloidal wave number $k_\theta \rho_i \gtrsim 1$.[26] Although their existence can influence the electron heat flux significantly, their impact on α particle transport is expected to be negligible due to the following reasons. With large spatial scale separation between α particle orbit and ETG wavelength, even stronger orbit-averaging and the frequency detuning[10,11] would occur compared to those for TEM. So, we focus our studies on TEM modes with $T_e = T_i$ in the wavelength regime, $k_\theta \rho_i \lesssim 1$. We use a poloidal wave number $k_\theta \rho_i = 0.34$ in the linear simulations, which is around the spectral peak of nonlinear simulation result. In addition, we use 32 grid points in one turn along the field line, and velocity space is discretized over 64 points in the parallel velocity and magnetic moment is discretized over 16 points in all simulations. The linear growth rates and real frequencies from GKW simulations are presented in Fig. 1. The real frequencies show mode propagation in the electron diamagnetic direction for all $k_\theta \rho_i$. This shows that input parameters can well present TEM mode relevant case. The TEM mode linear growth rate γ has a maximum around $k_\theta \rho_i = 0.8$.

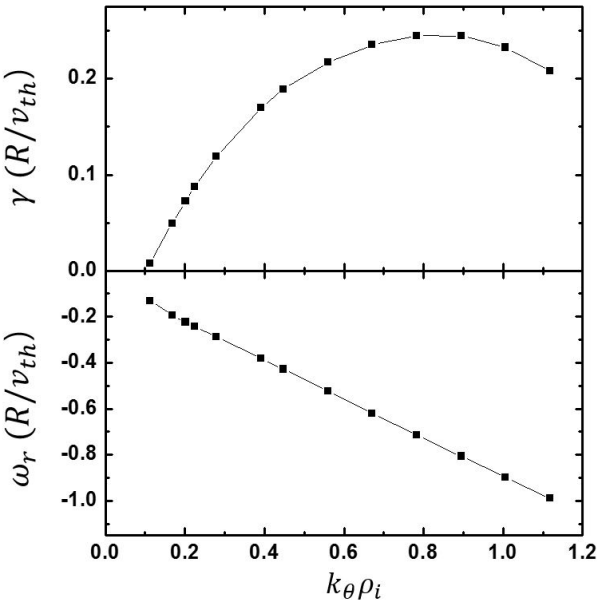

FIG. 1: Linear GKW calculations of the normalized real mode frequency and growth rate as functions of poloidal wavelength $k_\theta \rho_i$ for TEM CYLONE case.

Once the α particle concentrations are increased, two effects are expected in the linear simulations. First, α particles can contribute to the Poisson equation and affect to the growth rate. In order to investigate this effect, we set $R/L_{T\alpha} = 6.9$, $R/L_{n\alpha} = 2.2$ with fixed R/L_{ni}. The growth rate of the mode is rather insensitive to the variation of the α charge concentration up to 10% as shown in Fig. 2. This implies that we can treat alpha particle as passive tracer as explained in the previous section. This also implies that the stabilization of TEM by fast particles can be less important than that in ITG case in the electrostatic limit. Second, a presence of α particle can also lead to a change in R/L_{ni} due to the radial quasi-neutrality constraint. For example, alpha particle profiles based on the nominal ITER-FEAT parameters[27] are expected to have more peaked density profiles than main ion at r/a=0.5, $R/L_{n\alpha} = 20$.[14] So, R/L_{ni} should be changed consistently according

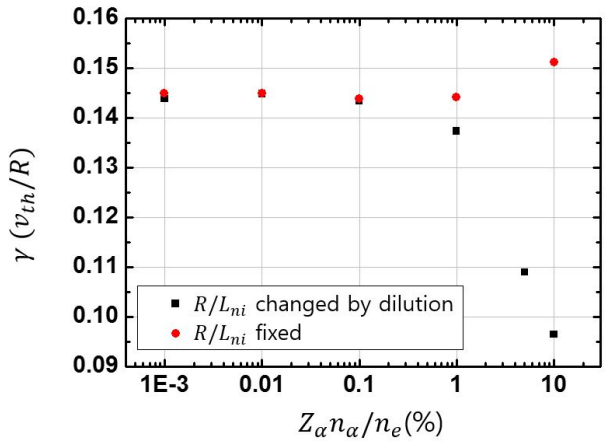

FIG. 2: Linear GKW calculations of normalized growth rate as a function of charge concentration with fixed R/L_{ni} (circles, red) and with changing R/L_{ni} (squares, black) due to dilution effect.

to the radial quasi-neutrality condition, $R/L_{ne} = \sum_s Z_s n_s R/L_{ns}$. In this case, a reduction of R/L_{ni} by increased α particle concentration would change the growth rate as shown in the Fig. 2. By comparing the result with fixed R/L_{ni}, we conclude that the change of the growth rate is dominated by the dilution effect. Note that the dilution effect is shown to be relatively small for 1% α-particle concentration in ITER, expected for standard scenarios based on Ref. 10 and 14.

We have computed the particle diffusion coefficient D_α in the quasilinear particle flux given in Eq. (17) and (18), as a function of E_α/T_e in Fig. 3. In Fig. 3, a reduction of the α particle transport as a function of E_α/T_e is demonstrated. This reduction could be understood with two effects according to the Eq. (18). One is the orbit-averaging effect, which is represented as the decrease of J_0 with increasing finite orbit width. And another is the frequency detuning effect, because only the relatively slow particles in the

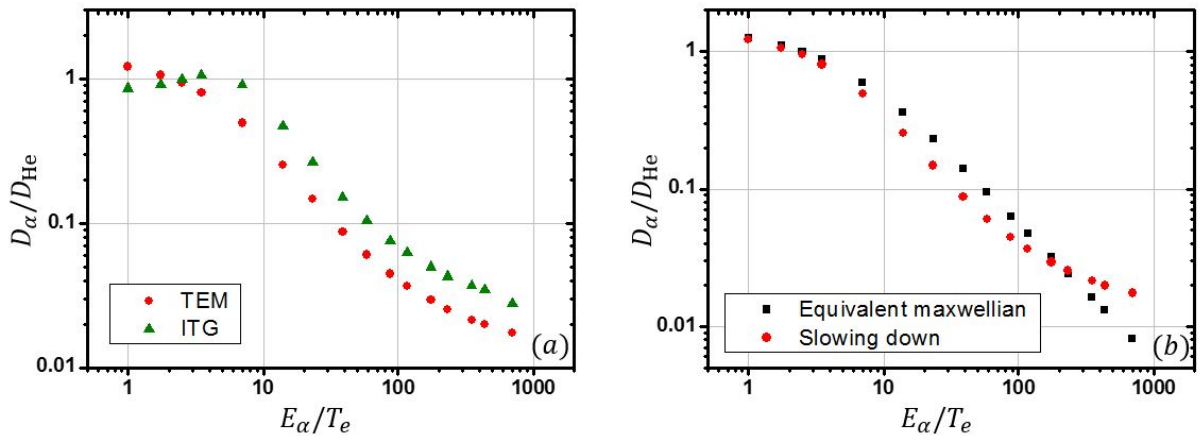

FIG. 3: The normalized diffusivity D_α/D_{He} of the α particles from linear GKW calculations for (a) the TEM (circles, red) and ITG (triangles, green) case and (b) the equivalent Maxwellian (squares, black) and the slowing down (circles, red) distribution as a function E_α/T_e .

velocity distribution function would satisfy the resonance conditions in the denominator, $\omega - k_\parallel v_\parallel - \omega_{d\alpha}$. A similar trend has been reported for ITG case.[10,11] This reduction is even stronger than that for ITG, due to shorter size of TEM as shown in Fig. 3 (a), where following parameters are chosen for ITG dominant case: $R/L_{Ti} = R/L_{Te} = 6.9$, $R/L_n = 3$, $k_\theta \rho_i = 0.34$.

A difference of D_α between the slowing-down and Maxwellian distribution case can be understood by comparing the population of slow particles which are transported more efficiently in the distribution function. In particular, the change of the 1D equilibrium distribution function (i.e. weighted by v^2) as a function of E_α/T_e is more appreciable for slowing down distribution function than for Maxwellian distribution function. Fig. 4 shows one example at two different E_α/T_e. For $E_\alpha/T_e = 350$, the slowing down distribution has more

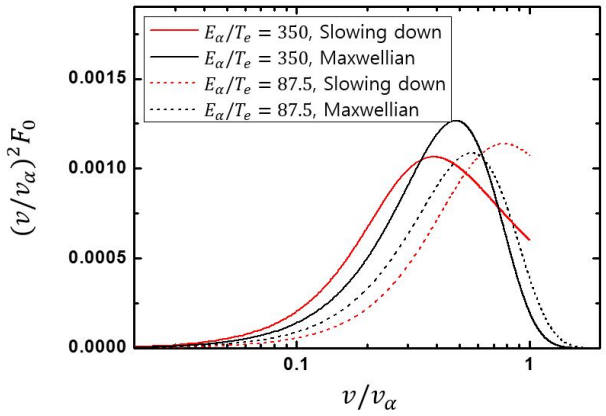

FIG. 4: A comparison of 1d slowing down F_s (red) and 1d Maxwellian F_M (black) distributions (weighted by $(v/v_\alpha)^2$) for $E_\alpha/T_e = 350$ (solid) and $E_\alpha/T_e = 87.5$ (short dash).

particles in the slow energy range than Maxwellian distribution. On the other hand, for $E_\alpha/T_e = 87.5$, the Maxwellian distribution has more particles in the slow energy range than the slowing down distribution. Therefore, for sufficiently high E_α/T_e, $E_\alpha/T_e > 300$, slowing down distribution has higher D_α than Maxwellian distribution while this trend would be reversed at lower E_α/T_e, $E_\alpha/T_e < 100$.

We also investigate thermodiffusion coefficients $C_{E\alpha} = D_{E\alpha}/D_\alpha$ given in Eq. (17) and (19) with respect to E_α/T_e in Fig. 5. A differences in $C_{E\alpha}$ between two different distribution function can be understood with the Eq. (19) where $K\left(\dot{E}\right)$ is given in Eqs. (11) and (13), respectively. For Maxwellian distribution, $C_{E\alpha}$ asymptotes to -3/2 in the limit of $T_e << E_\alpha$, while $C_{E\alpha}$ approaches to zero as $\dot{E}$ cancels out -3/2 in the opposite limit $T_e >> E_\alpha$ in Eq. (11). Then, a factor $dlnT_\alpha/dlnT_e$ has been multiplied for the equivalent Maxwellian distribution, where $dlnT_\alpha/dlnT_e$ approaches approximately to 0.2 for $T_e << E_\alpha$. For slowing down distribution, the level of $C_{E\alpha}$ is higher for the slowing down distribution function than

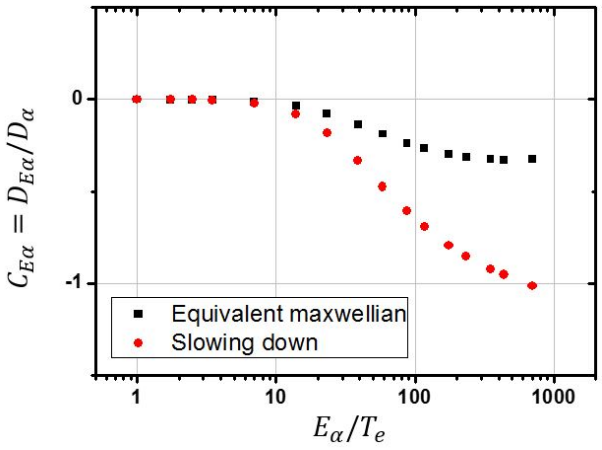

FIG. 5: The thermodiffusion coefficients $C_{E\alpha} = D_{E\alpha}/D_\alpha$ of the α particles from linear GKW simulations for the equivalent Maxwellian (squares, black) and the slowing down (circles, red) distribution as a function E_α/T_e.

for the equivalent Maxwellian. This is because $C_{E\alpha}$ in slowing down distribution strongly depends on the shape of the $K_s\left(\dot{E}\right)$, as already explained in Ref. 10.

$C_{p\alpha} = RV_{p\alpha}/D_\alpha$ is estimated to be small as shown in Fig. 6. This can be interpreted by Eq. (17) and (20) with the expressions of $H\left(\dot{E}\right)$ in Eqs. (10) and (12). For the Maxwellian distribution with $H_M\left(\dot{E}\right) = 1$, both outward and inward convection can occur depending on the value of E_α/T_e. An outward convection can be inferred as the contribution of $Re\,(\omega)$, while an inward convection can be understood as a contribution from $Im\,(\omega)$ related term in Eq. (20). This sign change of the $C_{p\alpha} = RV_{p\alpha}/D_\alpha$ with respect to E_α/T_e also happens for the slowing down distribution. However, an outward convection level around $T_e \approx E_\alpha$ is much lower than that for the Maxwellian distribution. This is because $H_s\left(\dot{E}\right)$ in Eq. (10) goes to zero as E_α/T_e approaches to 1.

A positive $C_{p\alpha}$ around $T_e \approx E_\alpha$ can be a consequence of the contribution of resonance

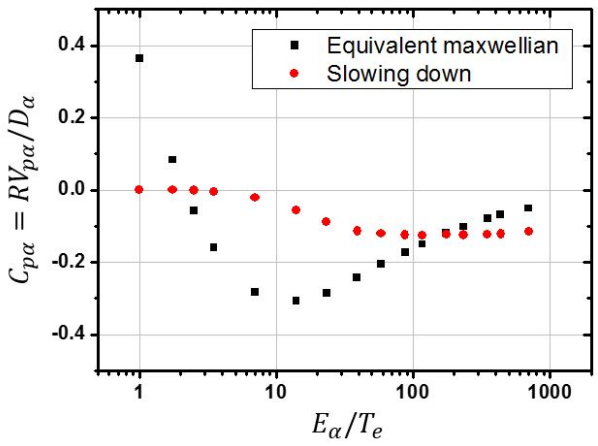

FIG. 6: The pure convection coefficients $C_{p\alpha} = RV_{p\alpha}/D_\alpha$ of the α particles from linear GKW simulations for the equivalent Maxwellian (squares, black) and the slowing down (circles, red) distribution as a function E_α/T_e at $k_\theta\rho_i \simeq 0.34$.

integral. Previous study considered the resonance condition in phase space for toroidal ITG in detail but without $k_\parallel$ related term.[28] In order to estimate the resonance condition, we have calculated $C_{p\alpha}$ and $k_\parallel v_\alpha / |\omega_r - \omega_{D\alpha}|$ at two different $k_\theta\rho_i$ as functions of E_α/T_e for Maxwellian distribution. Here, we have estimated $\omega_{d\alpha} \approx \omega_{D\alpha}$, ρ_α is estimated using v_α and $k_\parallel$ is approximated as $k_\parallel^{RMS}$ from the linear mode structure in the ballooning space. Note that the number of particles which can contribute to resonance integral is related to the ratio $k_\parallel v_\parallel / |\omega_r - \omega_{d\alpha}|$ because $\omega_r \propto \omega_{*e}$. Around $T_e \approx E_\alpha$, $k_\parallel v_\alpha > |\omega_r| > \omega_{D\alpha}$ is satisfied for the simulation results. For simplicity, we investigate a condition where the Landau resonances are dominant, then $C_{p\alpha}$ can be approximated as

$$C_{p\alpha} \approx -\omega_r/\omega_{D\alpha}. \tag{23}$$

An outward $C_{p\alpha}$ in a wider range of E_α/T_e at $k_\theta\rho_i = 0.2$ compared to the case at $k_\theta\rho_i = 0.34$ can be understood from the contribution of the resonance integral. As shown

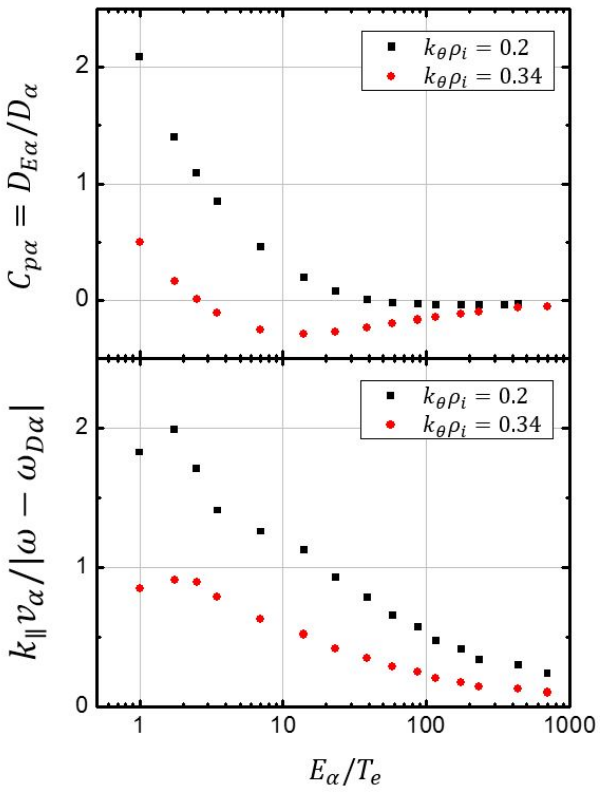

FIG. 7: The pure convection coefficients $C_{p\alpha} = RV_{p\alpha}/D_\alpha$ of the α particles from linear GKW simulations for the equivalent Maxwellian (squares, black) and the slowing down (circles, red) distribution as a function E_α/T_e.

in Fig. 7, at $k_\theta\rho_i = 0.2$, resonant integral can be more considerable than at $k_\theta\rho_i = 0.34$. On the other hand, for $E_\alpha >> T_e$, resonance integral becomes negligible and $C_{p\alpha}$ may be written as

$$C_{p\alpha} \approx -\omega_{D\alpha} \frac{\int \frac{F_\alpha J_0^2 \gamma}{\omega_{d\alpha}^2} d^3\mathbf{v}}{\int \frac{F_\alpha J_0^2 \gamma}{\omega_{d\alpha}} d^3\mathbf{v}}. \tag{24}$$

Here, only $Im\,(\omega) = \gamma$ related term remains in $C_{p\alpha}$, and this explains the inward convection around $T_e << E_\alpha$ at both $k_\theta\rho_i$.

IV. RESULTS FROM NONLINEAR SIMULATIONS

We have also performed a nonlinear simulation using the GKW code. The simulation parameters are the same as those of linear simulations. (i.e., $r/a = 0.5$, $R/a = 3$, $q = 1.4$, $s = 0.8$, $T_e = T_i$, $R/L_{Ti} = 2.2$, $R/L_{Te} = 6.9$ and $R/L_n = 2.2$) We consider a collisionless plasma in circular[29] geometry. Velocity space is discretized over 64 points in the parallel velocity and magnetic moment is discretized over 16 points in all simulations. The nonlinear simulations have been performed with 32 toroidal modes and 169 radial modes with a box size in the binormal and radial directions given by $L_y = 96.8\rho_i$ and $L_x = 65.6\rho_i$. In order to test the convergence of the simulation, we also carried out simulation with different radial box sizes and wavenumbers in the radial and binormal directions with two different cases in Table I. Figure 8 shows the results of convergence test with three different grid resolution. From figure 8 (a), we found that particle flux Γ_e is rather insensitive to grid resolution. However, electron heat diffusivity χ_e seems to be underestimated in case 1 as shown in figure 8 (b). On the other hand, case 2 and case 3 yield well converged results. We note that the case 3 has been used in previous studies with an acceptable convergence.[30] Therefore, we consider the grid resolution in case 2 to be adequate and use in the following sections for nonlinear runs.

The simulation exhibits a nonlinear saturation of fluctuation amplitude and fluxes after a brief linear growth phase as shown in Fig. 8. The expression for the α-particle flux in Eq. (17) is still valid in the nonlinearly saturated phase except for the fact that "ω" should now be interpreted as that in the nonlinear regime which includes possible broadening and

TABLE I: Radial box sizes and wavenumbers used for the convergence test of nonlinear simulations

	L_x	L_y	No. of toroidal mode	No. of radial mode	$(k_y\rho_i)_{max}$	$(k_x\rho_i)_{min}$
Case 1	$42.3\rho_i$	$62.4\rho_i$	21	169	2.52	15.60
Case 2	$65.6\rho_i$	$96.8\rho_i$	32	169	2.52	7.11
Case 3	$88.8\rho_i$	$131.1\rho_i$	43	339	2.52	14.94

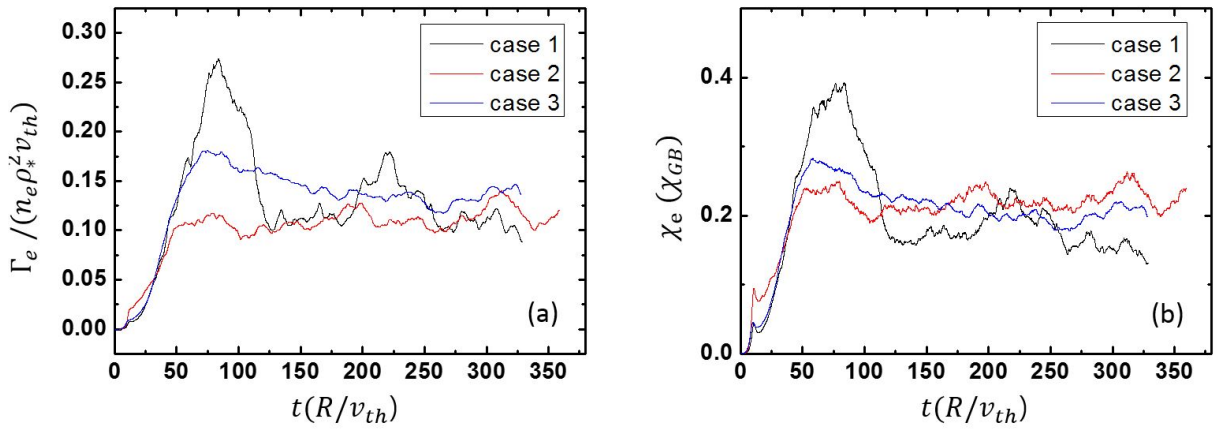

FIG. 8: The time evolution of electron particle flux, Γ_e, (a) and the normalized electron thermal diffusivity, χ_e, (b) from nonlinear GKW simulations with different grid resolutions with $\chi_{GB} = (\rho_s^2 c_s)/a$ with $c_s = (T_e/m_i)$ and $\rho_s = \frac{m_i c_s}{eB}$

shift. In addition. δf and $\delta\phi$ in that expression should exhibit values which are statistically constant in amplitudes.

While the main subject of this paper is α-particle transport, it is worthwhile to examine the fluctuation spectra at nonlinear saturation and discuss their relations to the expectations from the previous works. From the simulation data in the nonlinearly saturated phase, we

have obtained k_θ - spectrum of density fluctuation intensity $|\delta n/n_0|^2$. Although we don't purse a detailed nonlinear theory to be compared to that result, we compare the spectrum with an existing weak turbulence theory of CTEM which is based on the nonlinear gyrokinetic and bounce-kinetic equations[16] and the saturated amplitude with "mixing length" ansatz.

A formula from the mixing length ansatz can be obtained by arguing that a nonlinear saturation occurs when the linear drive is balanced by the nonlinear mode coupling. Usually a density evolution equation is used for drift wave turbulence drive by $\boldsymbol{\nabla} n_0$, this corresponds to balancing the linear drive term, $\delta \mathbf{u_E} \cdot \boldsymbol{\nabla} n_0$ to the nonlinear mode coupling term $\delta \mathbf{u_E} \cdot \boldsymbol{\nabla} \delta n$. If one ignores the difference between various $\mathbf{k}$'s appearing in the mode summation for the nonlinear mode coupling term in k-space, it leads to a familiar expression of

$$\frac{\delta n}{n_0} \simeq \frac{1}{k_r L_n}. \tag{25}$$

However, in our studies, CTEM is mainly driven by $\boldsymbol{\nabla} T_e$ rather than $\boldsymbol{\nabla} n_0$, although a small contribution of $\boldsymbol{\nabla} n_0$ exists which can be inferred from the dilution effect in Fig. 2. Therefore, we find Eq.(25) to be inapplicable to our case, and instead consider the trapped electron temperature evolution equation[31] which can be obtained by taking an energy moment of the bounce-kinetic equation.[32–34] Once again, by balancing the linear drive term $\delta \mathbf{u_E} \cdot \boldsymbol{\nabla} T_e$ to the $E \times B$ nonlinear mode coupling term $\delta \mathbf{u_E} \cdot \boldsymbol{\nabla} \delta T_e$, one can obtain an expression

$$\frac{\delta T_e}{T_e} \simeq \frac{1}{k_r L_{Te}}. \tag{26}$$

Associated density fluctuation level $\delta n/n_0$ can be estimated by balancing the $E\times B$ nonlinear coupling term in the trapped electron density evolution equation with the toroidal mode coupling term $\mathbf{v_{de}}\cdot\boldsymbol{\nabla}\delta T_e$ due to the energy-dependence of the trapped precession drift, we can get

$$\frac{|e|\,\delta\phi}{T_e}\cdot\left(\frac{\delta n}{n_0}\right)\simeq\frac{1}{k_rR}\frac{\delta T_e}{T_e}\simeq\frac{1}{k_r^2L_{Te}R}. \tag{27}$$

Further assuming $\delta n/n_0\simeq|e|\,\delta\phi/T_e$, we obtain

$$\frac{\delta n}{n_0}\simeq\frac{1}{k_r\sqrt{L_{Te}R}}. \tag{28}$$

This hybrid macroscopic length scale $(L_{Te}R)^{1/2}$ often appears in trapped particle driven turbulence.[34] Mixing length estimations in Eqs. (25), (26) and (28) are compared to the nonlinear result in Fig. 9. From these comparisons, we conclude a mixing length estimate using the trapped electron temperature evolution equation compares more favorably than the usual one from the density evolution equation. However, both are just useful rules of thumb and should not be considered as a substitute for a nonlinear theoretical estimation. In particular, the spectral transfer in k-space due to nonlinear mode coupling is not addressed in mixing length arguments.

There has been more detailed weak turbulence theory of CTEM[16] based on nonlinear gyrokinetic equations in which a saturated spectrum has been approximately calculated from the wave-kinetic equation. Here, we repeat the relevant formula from Eq. (27) of Ref. 16,

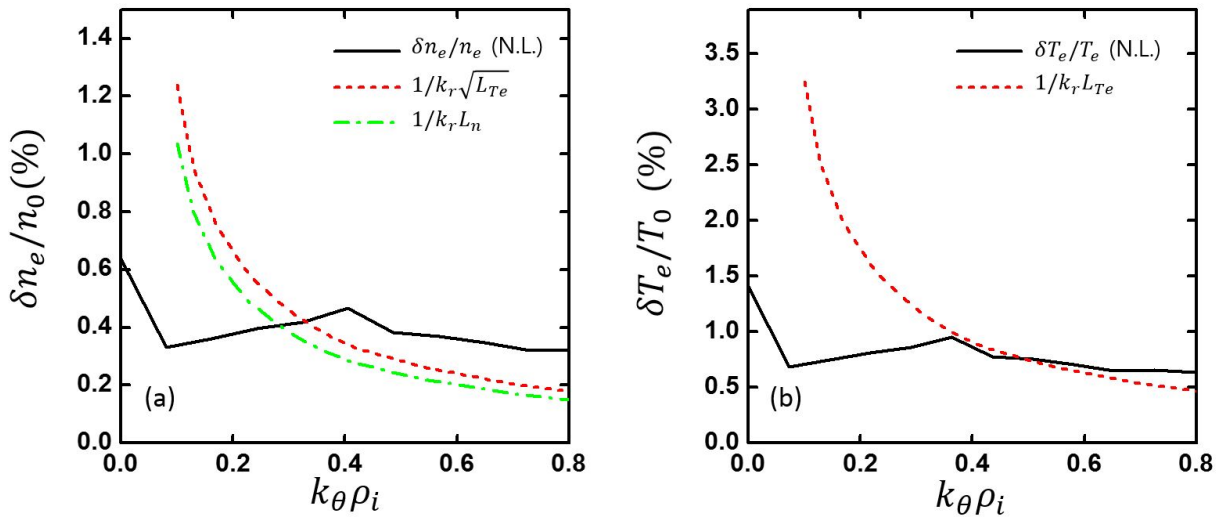

FIG. 9: $\delta n/n_0$ (a) and $\delta T_e/T_e$ (b) from nonlinear GKW simulations (solid, black) and its comparison to mixing length estimates ansatz, $1/k_r\sqrt{L_{Te}}$ (short dash, red) and $1/k_r L_n$ (dash dot, green) with ITER relevant gyro-radius, $\rho_i/a = 2.01 \times 10^{-3}$.

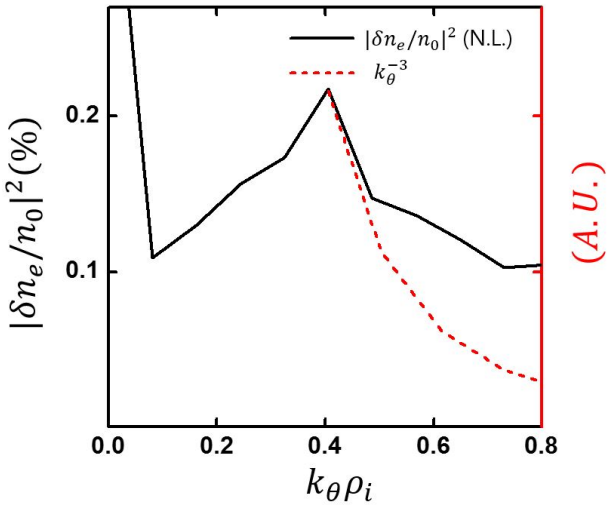

FIG. 10: $|\delta n/n_0|^2$ spectrum from nonlinear GKW simulations (solid, black) and its comparison to k_θ^{-3} (short dash, red) from weak turbulence theory with ITER relevant gyro-radius, $\rho_i/a = 2.01 \times 10^{-3}$.

$$\left|\frac{e\delta\phi}{T_e}\right|^2 \propto k_\theta^{-3}, \tag{29}$$

for $k_\theta \geq k_L$. $\left|\frac{e\delta\phi}{T_e}\right|$ is a rapidly increasing function of k_θ for $k_\theta \leq k_L$, and peaks at k_L. Here, $k_L^2\rho_s^2 \approx \frac{3(1+\eta_e)G}{\left(1+\frac{1+\eta_i}{\tau}\right)}\frac{L_n}{R}$. This formula is compared to the nonlinear simulation results in Fig. 10. Note that only the k-spectra shapes not the magnitudes of fluctuations are meaningful for comparison. We note that a prediction from Ref. 16 compares with the simulation result favorably for $k_\theta\rho_i \gtrsim 0.4$ with a caveat that a spectrum in Ref. 16 is for $\left|\frac{|e|\delta\phi}{T_e}\right|^2$, not for $|\delta n/n_0|^2$. Peak at $k_\theta\rho_i \lesssim 0.4$ results from a competition between the ion nonlinear damping (Compton scattering) and the trapped electron nonlinear damping (Compton scattering) according to Ref. 16. Notably, the density fluctuation spectra of Ohmic plasma in Tore Supra can be fitted by $|\delta n/n_0|^2 \propto k_\perp^{-\alpha}$, with $3 \leq \alpha \leq 3.5$ in the wavelength range, $0.5 \lesssim k_\perp\rho_i \lesssim 1$.[15] In the absence of the trapped electron nonlinearity, the spectrum would peak at a lower value of $k_\theta\rho_i$ as a result of inverse-cascade due to ion nonlinearity.[33,35] The trapped electron nonlinearity is kept in simulations and seems to play an important role in determining the spectral shape.

Now, we present the α-particle flux results from nonlinear simulation and compare with those from linear simulations. To isolate the pinch contribution to the α-particle transport, we have also performed nonlinear simulations with $R/L_{n\alpha} = 0$ and compared to a case with non-zero value of $R/L_{n\alpha}$. Here, Maxwellian distribution is used for α-particles. Fig. 11 (a) shows that the pinch part of energetic α particle flux is essentially zero. This is in contrast to the linear simulation results in which very small, but non-zero inward pinch

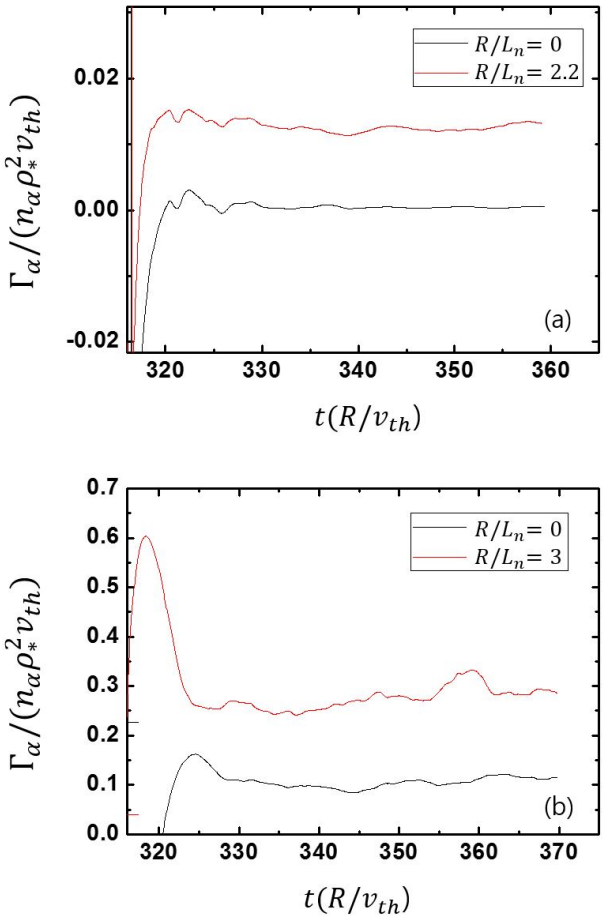

FIG. 11: The time evolution of normalized alpha particle flux, Γ_α, for energetic alpha ($E_\alpha/T_e = 175$) (a) and thermal Helium (b)

has been observed. Net energetic α-particle flux is outward and its corresponding effective diffusion coefficient is very small compared to that of the thermal He particles. This is consistent with the quasi-linear results shown in Fig. 3. On the other hand, the thermal He particle transport in Fig. 11 (b) exhibits a definite outward pinch, with a considerable net outward flux result for $R/L_{n\alpha} = 3$ (approximately 3 times the $R/L_{n\alpha} = 0$ result). We can speculate that a considerable He-ash accumulation at core will be unlikely in ITER due to this self-regulation of He ash profile.

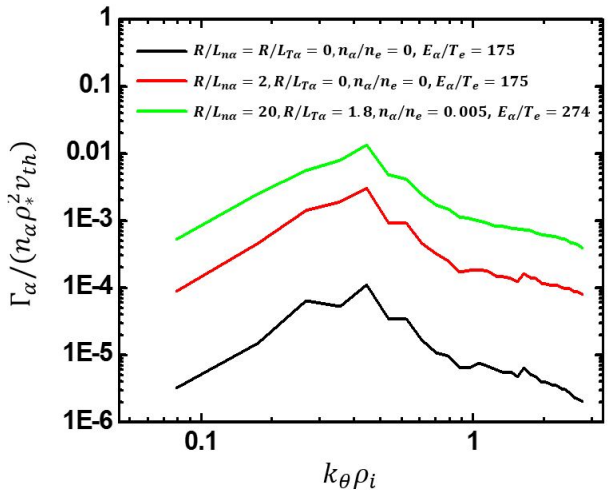

FIG. 12: α particle flux spectrum from nonlinear GKW simulations. Green line is obtained for parameters used in Ref. 14

Fig. 12 shows Γ_α from various modes at different logarithmic gradients. The contribution to Γ_α from various modes with different k_θ values are outward for all cases. A case with $R/L_{n\alpha} = 0$ and $R/L_{T\alpha} = 0$ clearly shows that the pure convection is outward for all k_θ values. This is somewhat different from the linear simulation result, where the inward convection was observed for $E_\alpha >> T_e$. However, the inward convection at $E_\alpha >> T_e$ is very small in the linear result, so the contribution from the resonant integral can change the result with nonlinear interaction with low k_θ. Also, Γ_α with $R/L_{n\alpha} = 0$ is much smaller than those from other cases with finite $R/L_{n\alpha}$. This clearly shows that contribution of pure convection is relatively smaller than diffusion for energetic alpha particles. Even larger Γ_α (green curve in Fig. 12) can be achieved with parameters considered in Ref. 14, while the increase of $R/L_{n\alpha}$ and $R/L_{T\alpha}$ is compensated by the increase of E_α/T_e which is closely related to orbit-averaging effect and the frequency detuning effect as already illustrated in the linear simulations. For all cases, a dominant contribution is from the modes with $k_\theta\rho_i \simeq 0.4$ where

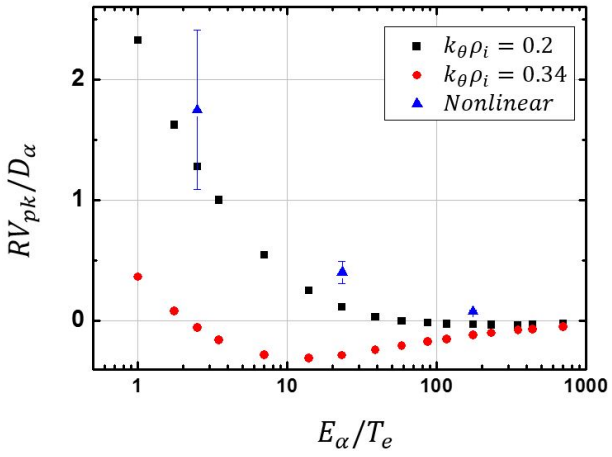

FIG. 13: The pure convection coefficients $C_{p\alpha} = RV_{p\alpha}/D_\alpha$ of the α particles from linear and nonlinear (blue, triangle) GKW simulations for the Maxwellian as a function E_α/T_e.

the spectral intensity in Fig. 12 also peaks.

Pure convection to diffusion ratio $C_{p\alpha} = RV_{p\alpha}/D_\alpha$ is shown in Fig. 13. Linear results from Fig. 7 (a) are repeated to facilitate a comparison. It shows that the pure convection is outward. The ratio is closer to that from a long wavelength ($k_\theta\rho_i \sim 0.2$) in the linear simulation, rather than that near the spectrum peak ($k_\theta\rho_i \sim 0.34$).

V. CONCLUSIONS

In this work, we have investigated transport of α particles due to TEM turbulence from nonlinear and quasilinear gyrokinetic simulations. We find that transport of α particles with high energy is significantly smaller than the thermal He transport and this this reduction is even stronger than that for ITG.[10] Pure convection of α particles from nonlinear simulation is outward and the convection to diffusion ratio decreases with E_α/T_e. In addition, k_θ spectrum

of $|\delta n/n_0|^2$ from nonlinear simulation shows a similar feature as those from experiments[15] and weak turbulence theory.[16]

In conclusion, we expect that α particles at high energy will be better confined than those at lower energy such as He-ash at core of ITER in the presence of TEM turbulence.

ACKNOWLEDGMENTS

This work was supported by the Ministry of Science, ICT and Future Planning of the Republic of Korea under the Korean ITER project contract. One of the Authors (S.M.Y.) would like to thank G.J. Choi for the fruitful discussions.

Appendix A

Reduced nonlinear toroidal electrostatic gyrokinetic equation used in this work can be obtained from the modern nonlinear gyrokinetic equation[8] as described below. The nonlinear gyrokinetic Vlasov equation for the total distribution function F of the guiding centers is given in Eq. (22a) with Eqs. (20) and (21) of Ref. 8. Note that the independent guiding center phase-space variables used in that formulation are $(\boldsymbol{R}, \mu, v_\parallel, \theta)$. After splitting F into $F_0 + \delta f$ where F_0 is the equilibrium distribution function which needs *not* to be a Maxwellian and δf is the perturbed part of the guiding center distribution function, we obtain

$$\begin{aligned}
&\{\frac{\partial}{\partial t} + \left(v_\parallel \mathbf{b} + \mathbf{v_D} + \frac{c\mathbf{b}}{B^*} \times \boldsymbol{\nabla} \langle \delta\phi \rangle\right) \cdot \boldsymbol{\nabla} - \frac{1}{m}\frac{\mathbf{B}^*}{B^*} \cdot \left(\mu \boldsymbol{\nabla} B + q \boldsymbol{\nabla} \langle \delta\phi \rangle\right) \frac{\partial}{\partial v_\parallel}\} \delta f \\
&= -\left(\frac{c\mathbf{b}}{B^*} \times \boldsymbol{\nabla} \langle \delta\phi \rangle + \mathbf{v_D}\right) \cdot \boldsymbol{\nabla} F_0 + \frac{\mathbf{B}^*}{mB^*} \cdot \left(\mu \boldsymbol{\nabla} B + q \boldsymbol{\nabla} \langle \delta\phi \rangle\right) \frac{\partial}{\partial v_\parallel} F_0. \qquad \text{(A1)}
\end{aligned}$$

where $\mathbf{v_D} = \frac{c\mathbf{b}}{B^*} \times \left(\frac{\mu}{q} \boldsymbol{\nabla} B + \frac{mcv_\parallel^2}{q} \mathbf{b} \cdot \boldsymbol{\nabla} \mathbf{b}\right)$, $\mathbf{B}^* = \mathbf{B} + \frac{mc}{q} v_\parallel \boldsymbol{\nabla} \times \mathbf{b}$, $\mathbf{B}^* = B^* \mathbf{b} + \frac{mcv_\parallel}{q} \mathbf{b} \times (\mathbf{b} \cdot \boldsymbol{\nabla})\, \mathbf{b}$, with $B^* = B + \frac{mc}{q} v_\parallel \mathbf{b} \cdot \boldsymbol{\nabla} \times \mathbf{b}$. B^* in the denominators of various expressions is related to the phase-space volume conservation and can be approximated by B in most cases including our studies with gradient-driven simulations, unless a long term simulation exceeding far beyond the nonlinear saturation phase is pursed. The last term on the LHS is the parallel velocity

space nonlinear term which is formally a higher order in nonlinear gyrokinetic ordering and also can be neglected in the same usual situations.

Note that in this representation, $\boldsymbol{\nabla} F_0$ has a contribution not only from $\boldsymbol{\nabla} n_0$ and $\boldsymbol{\nabla} T_0$, but also from $\boldsymbol{\nabla} B$ even for a Maxwellian F_0. Since most literature used the formulations where the free energy related $\boldsymbol{\nabla} n_0$ and $\boldsymbol{\nabla} T_0$ contributions to $\boldsymbol{\nabla} F_0$ eventually appear, it is useful to separate their contributions from that coming from $\boldsymbol{\nabla} B$. Using the chain rules for $\frac{\partial F_0}{\partial v_\parallel}$ with $E = \frac{1}{2} m v_\parallel^2 + \mu B$, one can show that $-\frac{c}{B}\mathbf{b} \times \boldsymbol{\nabla} \langle \delta\phi \rangle \cdot \boldsymbol{\nabla} F_0 = -\frac{c}{B}\mathbf{b} \times \boldsymbol{\nabla} \langle \delta\phi \rangle \cdot \boldsymbol{\nabla}_{\boldsymbol{p}} F_0 - \frac{c}{B}\mathbf{b} \times \boldsymbol{\nabla} \langle \delta\phi \rangle \cdot \mu \boldsymbol{\nabla} B \frac{\partial F_0}{\partial E}$. Then, the 2nd term from above, combined with the $c v_\parallel \mathbf{b} \times (\mathbf{b} \cdot \boldsymbol{\nabla})\, \mathbf{b} \cdot \boldsymbol{\nabla} \langle \delta\phi \rangle \frac{\partial F_0}{\partial v_\parallel}$ term contained in the last term on the RHS of Eq. (A1) yields $\mathbf{v_D} \cdot q \boldsymbol{\nabla} \langle \delta\phi \rangle \frac{\partial F_0}{\partial E}$. Finally, we obtain the following reduced equation for an *arbitrary* $F_0(E)$ which is *isotropic* in velocity space,

$$\begin{aligned} &\{\frac{\partial}{\partial t} + \left(v_\parallel \mathbf{b} + \boldsymbol{v}_D + \frac{c\mathbf{b}}{B^*} \times \boldsymbol{\nabla} \langle \delta\phi \rangle \right) \cdot \boldsymbol{\nabla} - \frac{b}{m} \cdot \mu \boldsymbol{\nabla} B \frac{\partial}{\partial v_\parallel} \} \delta f \\ &= -\left(\mathbf{v_D} + \frac{c}{B} \mathbf{b} \times \boldsymbol{\nabla} \langle \delta\phi \rangle \right) \cdot \boldsymbol{\nabla}_p F_0 + \left(v_\parallel \mathbf{b} + \mathbf{v_D} \right) \cdot q \boldsymbol{\nabla} \langle \delta\phi \rangle \frac{\partial F_0}{\partial E}. \end{aligned} \tag{A2}$$

Here, $\boldsymbol{\nabla}_{\boldsymbol{p}}$ refers to the gradient of F_0 only in terms of $\boldsymbol{\nabla} n_0$ and $\boldsymbol{\nabla} T_0$, not $\boldsymbol{\nabla} B$. Eq. (A2) of course reduces to the form which explicitly appears in an early version of GKW manual with Maxwellian F_0.[9]

In addition, by further splitting δf into the adiabatic part and non-adiabatic part, via $\delta f = \delta h - q \langle \delta\phi \rangle \frac{\partial F_0}{\partial E}$, one can also obtain Eq. (1) of Ref. 10. Note that in conventional gyrokinetic formulations[7,21] δh is defined in a particle phase space before transforming to the guiding center coordinates and performing gyrophase average. In modern gyrokinetics[8,17]

the order is reversed, and the "δf" in the Eqs. (A1), (A2) are defined in the guiding-center phase space. Therefore, $\langle \delta\phi \rangle$ rather than $\delta\phi$ appears in the definition of δh.

REFERENCES

[1]http://www.iter.org.

[2]Liu Chen and Fulvio Zonca, Physics of Alfvén waves and energetic particles in burning plasmas. *Reviews of Modern Physics*, 88(1), 2016.

[3]W. Tang, Microinstability theory in tokamaks . *Nuclear Fusion*, 18(8):1089, 1978.

[4]W. Horton, Drift waves and transport. *Reviews of Modern Physics*, 71(3):735–778, 1999.

[5]J. C. Adam, W. M. Tang, and P. H. Rutherford, Destabilization of the trapped-electron mode by magnetic curvature drift resonances. *Physics of Fluids*, 19(4):561–566, 1976.

[6]John D. Gaffey, Energetic ion distribution resulting from neutral beam injection in tokamaks. *Journal of Plasma Physics*, 16(02):149, oct 1976.

[7]E. A. Frieman and Liu Chen, Nonlinear gyrokinetic equations for low-frequency electromagnetic waves in general plasma equilibria. *Physics of Fluids*, 25(3):502–508, 1982.

[8]T. S. Hahm, Nonlinear gyrokinetic equations for tokamak microturbulence. *Physics of Fluids*, 31(9):2670–2673, 1988.

[9]A. G. Peeters, Y. Camenen, F. J. Casson, W. A. Hornsby, A. P. Snodin, D. Strintzi, and G. Szepesi. The nonlinear gyro-kinetic flux tube code GKW. *Computer Physics Communications*, 180(12):2650–2672, 2009.

[10]C. Angioni and A. G. Peeters. Gyrokinetic calculations of diffusive and convective transport of α particles with a slowing-down distribution function. *Physics of Plasmas*, 15(5), 2008.

[11]Wenlu Zhang, Zhihong Lin, and Liu Chen. Transport of energetic particles by microturbulence in magnetized plasmas. *Physical Review Letters*, 101(9):1–4, 2008.

[12]C. Angioni, A. G. Peeters, G. V. Pereverzev, A. Bottino, J. Candy, R. Dux, E. Fable, T. Hein, and R. E. Waltz. Gyrokinetic simulations of impurity, He ash and α particle transport and consequences on ITER transport modelling. *Nuclear Fusion*, 49(5), 2009.

[13]A. Di Siena, T. Görier, H. Doerk, J. Citrin, T. Johnson, M. Schneider, and E. Poli. Non-Maxwellian background effects in gyrokinetic simulations with GENE. *Journal of Physics: Conference Series*, 775(1), 2016.

[14]C. Estrada-Mila, J. Candy, and R. E. Waltz. Turbulent transport of alpha particles in reactor plasmas. *Physics of Plasmas*, 13(11), 2006.

[15]P. Hennequin, R. Sabot, C. Honoré, G. T. Hoang, X. Garbet, A. Truc, C. Fenzi, and A. Quéméneur, Scaling laws of density fluctuations at high-k on Tore Supra. *Plasma Physics and Controlled Fusion*, 46(12 B), 2004.

[16]T. S. Hahm and W. M. Tang, Weak turbulence theory of collisionless trapped electron driven drift instability in tokamaks. *Physics of Fluids B*, 3(4):989–999, 1991.

[17]A. J. Brizard and T. S. Hahm, Foundations of nonlinear gyrokinetic theory. *Reviews of Modern Physics*, 79(2):421–468, 2007.

[18]T. S. Hahm, Nonlinear gyrokinetic equations for turbulence in core transport barriers. *Physics of Plasmas*, 3(12):4658–4664, 1996.

[19]Alain J. Brizard, Nonlinear gyrokinetic Vlasov equation for toroidally rotating axisymmetric tokamaks. *Physics of Plasmas*, 2(2):459–471, 1995.

[20]H. Sugama and W. Horton, Nonlinear electromagnetic gyrokinetic equation for plasmas

with large mean flows. *Physics of Plasmas*, 5(7):2560–2573, 1998.

[21]P. J. Catto, W. M. Tang, and D. E. Baldwin, Generalized gyrokinetics. *Plasma Physics*, 23(7):639 to 650, 1981.

[22]J. W. Connor, R. J. Hastie, and J. B. Taylor, Shear, periodicity, and plasma ballooning modes. *Physical Review Letters*, 40(6):396–399, 1978.

[23]Mike Kotschenreuther, G. Rewoldt, and W. M. Tang, Comparison of initial value and eigenvalue codes for kinetic toroidal plasma instabilities. *Computer Physics Communications*, 88(2-3):128–140, 1995.

[24]A. M. Dimits, G. Bateman, M. A. Beer, B. I. Cohen, W. Dorland, G. W. Hammett, C. Kim, J. E. Kinsey, M. Kotschenreuther, A. H. Kritz, L. L. Lao, J. Mandrekas, W. M. Nevins, S. E. Parker, A. J. Redd, D. E. Shumaker, R. Sydora, and J. Weiland, Comparisons and physics basis of tokamak transport models and turbulence simulations. *Physics of Plasmas*, 7(3):969–983, 2000.

[25]G. Rewoldt, Z. Lin, and Y. Idomura, Linear comparison of gyrokinetic codes with trapped electrons. *Computer Physics Communications*, 177(10):775–780, 2007.

[26]T. Vernay, S. Brunner, L. Villard, B. F. McMillan, S. Jolliet, A. Bottino, T. Görler, and F. Jenko, Global gyrokinetic simulations of TEM microturbulence. *Plasma Physics and Controlled Fusion*, 55(7), 2013.

[27]D. J. Campbell, The physics of the International Thermonuclear Experimental Reactor FEAT. *Physics of Plasmas*, 8(5 II):2041–2049, 2001.

[28]A. Di Siena, T. Görler, H. Doerk, E. Poli, and R. Bilato, Fast-ion stabilization of tokamak plasma turbulence. *Nuclear Fusion*, 58(5), 2018.

[29]X. Lapillonne, S. Brunner, T. Dannert, S. Jolliet, A. Marinoni, L. Villard, T. Görler, F. Jenko, and F. Merz, Clarifications to the limitations of the s-α equilibrium model for gyrokinetic computations of turbulence. *Physics of Plasmas*, 16(3), 2009.

[30]C. Angioni, R. Bilato, F. J. Casson, E. Fable, P. Mantica, T. Odstrcil, M. Valisa, and ASDEX Upgrade Team JET Contributors, Gyrokinetic study of turbulent convection of heavy impurities in tokamak plasmas at comparable ion and electron heat fluxes. *Nuclear Fusion*, 57(022009), 2017.

[31]Michael Alan Beer, Gyrofluid Models of Turbulent Transport in Tokamaks. *PhD thesis, Prnceton University*, 43(January):196, 1995.

[32]F. Y. Gang, P. H. Diamond, and M. N. Rosenbluth, A kinetic theory of trapped-electron-driven drift wave turbulence in a sheared magnetic field. *Physics of Fluids B*, 3(1):68–86, 1991.

[33]Liu Chen, L Berger, and J G Lominadze, Nonlinear Saturation of the Dissipative Trapped-Electron Instability. *Physical Review Letters*, 39(12), 1977.

[34]T. S. Hahm and W. M. Tang, Nonlinear theory of collisionless trapped ion modes. *Physics of Plasmas*, 3(1):242–247, 1996.

[35]P. L. Similon and P. H. Diamond, Nonlinear interaction of toroidicity-induced drift modes. *Physics of Fluids*, 27(4):916–924, 1984.